https://doi.org/10.5194/angeo-2019-103
Preprint. Discussion started: 19 July 2019
© Author(s) 2019. CC BY 4.0 License.

Annales Geophysicae Discussions

# Plasma transport into the duskside magnetopause caused by Kelvin-Helmholtz vortices in response to the northward turning of the interplanetary magnetic field observed by THEMIS

Guang Qing Yan[1], George K. Parks[2], Chun Lin Cai[1], Tao. Chen[1], James P. McFadden[2], Yong Ren[1,3]

[1] State Key Laboratory of Space Weather, National Space Science Center, Chinese Academy of Sciences, Beijing, China, 100190

[2] Space Science Laboratory, University of California, Berkeley, California, USA, CA94720

[3] University of Chinese Academy of Sciences, Beijing, China, 100049

**Abstract: A train of Kelvin-Helmholtz (K-H) vortices with plasma transport across the magnetopause has been observed by the Time History of Events and Macroscale Interactions during Substorms (THEMIS) when the interplanetary magnetic field (IMF) abruptly turns northward. This unique event occurred without pre-existing denser boundary layer to facilitate the instability. Two THEMIS spacecraft, TH-A and TH-E, separated by 3 Re, periodically encountered the duskside magnetopause and the low-latitude boundary layer (LLBL) with a period of 2 minutes and tailward propagation of 194 km/s. There was no high-velocity low-density feature, but the rotations in the bulk velocity observation, distorted magnetopause with plasma parameter fluctuations and the magnetic field line stretching, indicate the formation of rolled-up K-H vortices at the duskside magnetopause. A mixture of magnetosheath ions with magnetospheric ions and enhanced energy flux of hot electrons is identified in the K-H vortices. This mixture region appears more periodic at the upstream spacecraft and more dispersive at the downstream location, indicating a significant transport can occur and evolve during the tailward propagation of the K-H waves. There is still much work to fully understand the Kelvin-Helmholtz mechanism. The observations of direct response to the northward turning of the IMF, the unambiguous plasma transport within the vortices, involving both ion and electron fluxes can provide additional clues to the K-H mechanism.**

**Key words**: K-H vortices, northward IMF, plasma transport, LLBL

https://doi.org/10.5194/angeo-2019-103
Preprint. Discussion started: 19 July 2019
© Author(s) 2019. CC BY 4.0 License.

Annales Geophysicae Discussions

## 1 Introduction

Kelvin-Helmholtz (K-H) instability can be activated at the interface between different plasma regimes with different velocities, and the perturbations propagate along the direction of the velocity shear as a form of surface wave developing into nonlinear vortices. As shown by Hasegawa (1975), the high density and the magnetic field perpendicular to the velocity shear on either side of the interface facilitate the unstable condition. The fastest K-H instability occurs when the wave vector ***k*** is parallel/antiparallel to the velocity shear and perpendicular to the magnetic field (Southwood, 1979; Manuel & Samson, 1993). This condition favors the low-latitude magnetopause where the velocity shear and the northward magnetospheric magnetic field are available. The magnetic tension stabilizes the shear layer if the magnetic field and the velocity shear are aligned, indicating that the radial IMF does not favor the K-H instability. However, reported observation indicates that K-H waves occur at the high-latitude magnetopause under the dawnward IMF and continues to exist when the IMF turns radial (Hwang et al., 2012). On the other hand, under the radial IMF, K-H instability is found in both simulations (Tang et al., 2013; Adamson et al., 2016) and observations (Farrugia et al., 2014; Grygorov et al., 2016). In some cases, the K-H instability is thought facilitated by a denser boundary layer formed by the dayside magnetic reconnections (Grygorov et al., 2016), by the plasma plume (Walsh et al., 2015), or by the pre-existing denser boundary layer formed by the high-latitude reconnections under the northward IMF (Hasegawa et al., 2009; Nakamura et al. 2017). Theoretically, both northward and southward IMF can favor the K-H instability at the low-latitude magnetopause. In fact, almost all of the previous observations (Chen & Kivelson, 1993; Kivelson & Chen, 1995; Fujimoto et al., 2003; Hasegawa et al., 2004) and simulations (Chen et al., 1997; Farrugia et al., 2003; Miura, 1995; Hashimoto & Fujimoto, 2005) show that the K-H waves occur preferentially under the northward IMF, although linear K-H waves are observed under the southward IMF (Mozer et al., 1994; Kawano et al., 1994). However, under the southward IMF, Cluster has observed nonlinear K-H waves with irregular and turbulent characteristics (Hwang et al., 2011) and THEMIS has observed regular K-H vortices with an induced electric field at the edges (Yan et al., 2014). Recently, a statistical survey indicates that K-H waves are much more ubiquitous than previously thought (Kavosi & Raeder, 2015), which implies the importance of the solar wind plasma transport into the magnetosphere via the K-H vortices.

In addition to magnetic reconnections at low latitude (Dungey, 1961) and high latitude magnetopause (Song & Russell, 1992), whose nature is a popular research topic (e.g., Dai, 2009; Dai et al., 2017; Dai, 2018), the K-H instability is an important way to transport solar wind into the magnetosphere when reconnections are inactive at the magnetopause. A statistical study of Double Star observations implies the entry of cold ions into the flank magnetopause caused by the K-H vortices that is enhanced by solar wind speed (Yan et al., 2005). However, it is noted that the K-H instability itself cannot lead to plasma transport across the magnetopause (Hasegawa et al., 2004); therefore, certain secondary processes (e.g., Nakamura et al., 2004; Matsumoto & Hoshino, 2004; Chaston et al., 2007) are necessarily coupled with the K-H instability for plasma transport into the magnetosphere via the LLBL. The reconnection of the twisted magnetic field lines inside the K-H vortex was first found in a simulation (Otto & Fairfield, 2000) and has since been identified in observations (Nykyri et al., 2006; Hasegawa et al., 2009; Li, et al., 2016). The plasma transport into the magnetosphere via such a process in K-H vortices has been quantitatively

https://doi.org/10.5194/angeo-2019-103
Preprint. Discussion started: 19 July 2019
© Author(s) 2019. CC BY 4.0 License.


investigated in a simulation (Nykyri & Otto, 2001). Most recently, energy transport from a K-H wave into a magnetosonic wave was estimated conserving energy in the cross-scale process, and three possible ways were discussed to transfer energy involving shell-like ion distributions, kinetic Alfvén waves, and magnetic reconnection (Moore et al., 2016). Up to now, reports of direct observations of plasma transport in the K-H vortices are only a hand full (e.g., Sckopke et al., 1981; Fujimoto et al., 1998; Hasegawa et al., 2004). Moreover, the microphysical processes for the plasma transport remains unclear, indicating more observations of such a transport process are needed to help us understand the physics. In this work, we present the THEMIS observations of the K-H vortices activated when the IMF abruptly turns northward, without a pre-existing denser boundary layer to facilitate the instability. We show a significant solar wind transport into the magnetosphere occurs and evolves within the vortices.

## 2 Data and Methods

The THEMIS mission (Angelopoulos, 2008) consists of five identical spacecraft originally orbiting the Earth similar to a string of pearls configuration. In August 2009, TH-B and TH-C were pushed to the vicinity of the lunar orbit, while the other three stayed in the near-Earth orbit with an apogee of approximately 13 Re. The instruments onboard include a flux gate magnetometer (FGM) (Auster et al., 2008) to measure the magnetic field and an electrostatic analyzer (ESA) (McFadden et al., 2008) to measure the electron (6 eV-30 keV) and ion (5 eV-25 keV) fluxes. We used the 3-second averaged FGM and ESA data from TH-A and TH-E to perform the particle analysis, and the 1/16 second averaged FGM data to perform the minimum variance analysis (MVA) (Sonnerup & Cahill, 1968) to determine the local magnetopause coordinates to find the distortions of the magnetopause. The FGM and ESA data from TH-B located in the dawnside downstream solar wind provide the IMF and solar wind conditions with an estimated time lag of 10 minutes from the subsolar magnetopause to TH-B. Both ion and electron energy spectra with a 3-second resolution were used to diagnose the mixture of the magnetosheath and magnetospheric ions. During the interval of interest, there are no data in the top energy channels centered at 25.21 keV for the ion spectrum and 31.76 keV for the electron spectrum, which has not influenced our investigations.

## 3 Observations and Discussions

During the interval UT 22:20-22:54 on March 28, 2016, TH-A and TH-E were located near the magnetopause (figure 1), while TH-D was located in the inner magnetosphere, far from the magnetopause. TH-B, near the lunar orbit, was immersed in the solar wind at the dawnside downstream of the other two spacecraft. As shown in panel 1 of figure 3, TH-B observed an abrupt turning of the IMF from duskward to northward at UT 22:32, corresponding to UT 22:22, with a time lag of 10 minutes ((10+32.7) Re / (450 km/s)) from the subsolar magnetopause to TH-B. Periodical fluctuations were observed in both the TH-A and TH-E observations (figure 2), from ion density in panel 1, temperature in panel 2, magnetic field in panel 3 and 7, to velocity in panel 4 and 8, especially the alternating appearances of hot and cold ions in the energy-time spectra (panel 5 and 9). The period was approximately 2 minutes (17 peaks within 34 minutes), and the tailward bulk propagation speed was approximately 195 km/s (3 Re / 90 s). In figure 3, the rotational characteristics were identified in the periodical fluctuations in $V_l$, $V_m$ and $V_n$ with phase differences between them. The magnetic field deviations in panels 3 and 5 indicated the stretching of the magnetic field along with the deformation of the magnetopause. The alternating appearances of the two different plasmas imply the multiple periodic encounters of the magnetopause and the LLBL, which is one of the typical characteristics of K-H vortices.

At UT 22:24, UT 22:32, UT 22:36, UT 22:39, marked by the black arrows, TH-A observed magnetosheath cold ions without magnetospheric hot ions (green regions at top of panel 5, figure 2). The absence of hot ions indicated that the spacecraft had crossed the magnetopause into the magnetosheath, where the outbound and inbound crossings of the magnetopause can be identified. At each pair of traversals, the local magnetopause coordinates LMN were calculated by using MVA (Sonnerup & Cahill, 1968). The calculated normal direction ***N*** as well as the parallel direction ***M*** of the local magnetopause is used to identify the distorted magnetopause. In each panel of figure 4, the normal and parallel directions ***M-N*** at the outbound and inbound magnetopause are plotted in the equatorial plane, compared with the average ***M-N*** of the magnetopause. The average magnetopause in dotted line, as well as the average ***M-N*** directions, is calculated from the model (Shue, 1998), and the dotted line is also approximately the trajectory of the spacecraft TH-A, which is moving at a relatively slow speed of about 2 km/s at the apogee. The distorted magnetopause is plotted in black line, perpendicular to ***N*** and parallel to ***M*** at outbound and inbound. The deviations of the ***M-N*** directions from the averaged magnetopause illustrate the magnetopause distortions formed by the K-H vortices. Such distortions of the magnetopause qualitatively explain the periodically alternating encounters of magnetosphere-like and magnetosheath-like plasmas. The plasma rotation is also illustrated by the red circle with arrow, consistent with the observation in panel 4 of figure 2.

The high-speed low-density feature is one of the characteristics of rolled-up vortices (Hasegawa et al., 2006), but not for every event (Masson & Nykyri, 2016), because the acceleration occurs only in certain stages of the development. Figure 5 shows the $V_m$-$N_i$ plot, in which the blue lines mark the high-speed and low-density region. $V_m$ is the tailward velocity, the M component of the measured velocity expressed in the averaged magnetopause coordinates LMN. In this event, there are few measurements distributed in the high-speed and low-density region, indicating that the high-speed and low-density feature was not seen in the $V_m$-$N_i$ plot (figure 5). However, the rotations of the plasma flows, the stretching of the magnetic field lines, and the distortions of the magnetopause indicated the formation of rolled-up K-H vortices. It is worth noting that the first peak arrived as soon as the IMF turned northward at UT 22:22, while no pre-existing denser boundary layer resulting from high latitude reconnections was needed to facilitate the K-H instability as previously described (Hasegawa et al., 2009; Nakamura et al. 2017).

Before and after the UT 22:22-22:52 interval, the magnetospheric hot ions dominated in panel 5 of figure 2, mainly in the 5-25 keV range with an energy flux of $10^6$ eV/(cm$^2$-s-sr-eV), and the magnetospheric hot electrons dominated in panel 6, mainly in the 0.5-25 keV range with an energy flux of over $10^7$ eV/(cm$^2$-s-sr-eV). On the other hand, during the UT 22:22-22:52 interval, the repeating magnetosheath cold ions in panel 5 were primarily observed between 0.1-3 keV with an energy flux of over $10^6$ eV/(cm$^2$-s-sr-eV), and the cold electrons in panel 6 were observed between 10-500 eV, with an energy flux of over $10^7$ eV/(cm$^2$-s-sr-eV). Embedded in the plasmas of the two different origins, the coexisting hot and cold ions overlapped. The alternating shifts of the hot and cold ions appeared more periodic at the upstream location of TH-A (panel 5 in figure 2), but more dispersed at the downstream TH-E. Taking the mass ratio of protons to electrons into

https://doi.org/10.5194/angeo-2019-103
Preprint. Discussion started: 19 July 2019
© Author(s) 2019. CC BY 4.0 License.


account, the gyro-radius of the electrons is only 1/42 of protons with the same energy and the same magnetic field, estimated to be approximately 2 km. We understand the ion mixture/transport as the observed substantial magnetosheath ions in the steady background of the magnetospheric plasma (and vice versa). For the proton's gyro-radius of approximately 80-100 km at the magnetopause, the coexistence of the hot and cold ions in the spectrum is not sufficient to diagnose the mixture of the two components. Thus, we used the observed hot electrons as an additional indicator of the magnetosphere region because of their relatively smaller gyro-radius. Hence, the criteria to identify the mixture/transport are described such that the cold ions of 0.1-3 keV can be observed with an energy flux over $10^5$ eV /(cm$^2$-s-sr-eV) in the hot ions background, with an energy flux over $10^6$ eV /(cm$^2$-s-sr-eV), as well as a substantial enhancement in the energy flux of the hot electrons of 0.5-5 keV. Based on such criteria, the ion mixture/transport intervals were diagnosed from both TH-A and TH-E, marked by the green bars at the bottom of panel 6 and the black bars at the bottom of panel 10 in figure 2. The transport regions in the TH-A observations were distributed at the edges of the vortices and appeared to be more periodic, while the TH-E observations were more dispersive. This feature was also found in the alternating encounters of the magnetosheath and magnetosphere ions in the spectra (panels 5 & 9 in figure 2). This outcome means that substantial solar wind transport into the magnetosphere occurred during the tailward propagation from TH-A to TH-E. As mentioned above, the first K-H wave, as well as the mixture regions arrived at the upstream TH-A as soon as the IMF abruptly turned northward. The K-H vortices were evidently activated as a response to the abrupt northward turning of the IMF, and no pre-existing denser boundary layer resulting from the high latitude reconnections was needed to facilitate the K-H instability.

Previously, both electron and ion distributions were used to diagnose the region of observation (Chen et al., 1993). While diagnosing the mixture/transport regions in this event, the typical plasma features in different regions were selected for comparisons (figure 6), as illustrated by the energy flux distributions of both ions (blue line) and electrons (red line). In panels 1, both the ion and electron fluxes show single-peak at the low energy, indicating the components of cold and dense magnetosheath plasma. In panel 2, the ion flux shows a double-peak, which means the coexistence of the magnetosheath cold ions and magnetospheric hot ions. The relatively smaller peak/enhancement in the electron flux show that the magnetospheric hot electrons are detected, but the cold electrons dominate, implying the spacecraft is located in magnetosheath but very close to the magnetospause, a mixture region. In panel 3, both the ion and electron fluxes show double-peak. The double-peak of the ion flux indicates co-existence of the magnetosheath cold ions and magnetospheric hot ions. For the electron flux, the peak at the high energy indicates that more magnetospheric hot electrons are detected, implying that the spacecraft is located in magnetosphere, another example of mixture region. In panel 4, both ion and electron fluxes show single-peak at the high energy, indicating the components of hot and tenuous magnetospheric plasma. It should be noted that the ion flux plots (blue lines in each panel) should be lower in the tail, but show no such decrease tails in part because the data were absent at the high energy channels. The typical regions shown correspond to the magnetosheah, the energetic particle streaming layer, the LLBL, and the magnetosphere (Sibeck, 1991).

## 4 Summary

We analyzed observations from TH-A and TH-E that periodically encountered the LLBL; the

© Author(s) 2019. CC BY 4.0 License.


K-H vortices were identified by the rotation features in the bulk velocity, magnetic field deviations indicating the field line stretching, and the distortions of the magnetopause deduced by MVA, which indicate the generation of K-H vortices, without the high-speed low-density features. The K-H vortices started as soon as the IMF turned northward abruptly, without any pre-existing denser boundary layer formed by high-latitude reconnections to facilitate the instability. By considering the enhancement of the hot electrons as an indicator of the magnetosphere region, the ion mixture/transport regions were shown that significant plasma transport can occur during the tailward propagation from TH-A to TH-E. Typical plasma features were observed in different regions. These new observations characterized by the direct response to the northward turning of the IMF, the unambiguous plasma transport involving both ion and electron fluxes, complement existing observations and help further our understanding of the plasma transport processes in K-H vortices.

## Acknowledgements

This work was supported by the Strategic Pioneer Program on Space Science, Chinese Academy of Sciences, Grant No. XDA15052500, XDA15350201, and XDA17010301, and by the National Natural Science Foundation of China, Grant No. 41574161, 41731070, 41574159 and 41004074. The data for this paper are available at the Coordinated Data Analysis Web of NASA's Goddard Flight Center (http://cdaweb.gsfc.nasa.gov/istp_public/). The authors are grateful to NASA's Goddard Flight Center and the associated instrument teams for supplying the data. The Authors thank Professor Chi Wang and Professor Lei Dai for valuable scientific discussions. The authors also express their thanks for the support from the Specialized Research Fund for State Key Laboratories and the CAS-NSSC-135 project. Part of the work was done during G. Q. Yan's visit at UC Berkeley, who cordially appreciates the assistance from Professor Forrest S. Mozer.

## References

Adamson, E., Nykyri, K., and Otto, A.: The Kevin-Helmholtz instability under Parker-Spiral interplanetary Magnetic Field conditions at the magnetospheric flanks, Adv. Space Res., 58, 218-230, 2016.

Angelopoulos, V.: The THEMIS mission, Space Sci. Rev., 141, 5–34, doi:10.1007/s11214-008-9336-1, 2008.

Angelopoulos, V., The ARTEMIS mission, Space Sci. Rev., 165, 3–25, doi:10.1007/s11214-010-9687-2, 2011.

Auster, U., Glassmeier, K. H., Magnes, W., Aydogar, O., Baumjohann, W., Constaninescu, D., Fischer, D., Fornicon, K. H., Georgescu, E., Harvey, P., Hillenmaier, O., Kroth, R., Ludlam, M., Narita, Y., Nakamura, R., Okrafca, K., Plaschke, F., Richter, I., Schwartzl, H., Stoll, B., Vanavanoglou, A., Wiedemann, M.: The THEMIS fluxgate magnetometer, Space Sci. Rev., 141, 235–264, doi:10.1007/s11214-008-9365-9, 2008.

Chaston, C. C., Wilber, M., Mozer, F. S., Fujimoto, M., Goldstein, M. L., Acuna, M., Rème, H., and Fazakerley, A.: Mode conversion and anomalous transport in Kelvin-Helmholtz vortices and kinetic Alfven waves at the Earth's magnetopause, Phys. Rev. Lett., 99, 175004, Doi: 10.1103/PhysRevLett.99.175004, 2007.

© Author(s) 2019. CC BY 4.0 License.

Chen, Q., Otto, A., and Lee, L. C.: Tearing instability, Kelvin-Helmholtz instability, and magnetic reconnection, J. Geophys. Res., 102(A1), 151-161, 1997.

Chen, S. H., and Kivelson, M. G.: On nonsinusoidal waves at the magnetopause, Geophys. Res. Lett., 20, 2699-2702, 1993.

Chen, S.-H., Kivelson, M. G., Gosling, J. T., Walker, R. J., and Lazarus, A. J.: Anomalous aspects of magnetosheath flow and of the shape and oscillations of the magnetopause during an interval of strongly northward interplanetary magnetic field, J. Geophys., 98, 5727-5742, 1993.

Dai, L.: Collisionless Magnetic Reconnection via Alfven Eigenmodes, Phys. Rev. Lett., 102, 245003, doi:https://doi.org/10.1103/PhysRevLett.102.245003, 2009.

Dai, L., Wang, C., Zhang, Y., Lavraud, B., Burch, J., Pollock, C., and Torbert, R. B.: Kinetic Alfvén wave explanation of the Hall fields in magnetic reconnection, Geophys. Res. Lett., 44, 634–640, doi:10.1002/2016GL071044, 2017.

Dai, L.: Structures of Hall Fields in Asymmetric Magnetic Reconnections, J. Geophys. Res. Space Physics, 123(9), 7332-7341, doi: https://doi.org/10.1029/2018JA025251, 2009.

Dungey, J. W.: Interplanetary magnetic field and auroral zones, Phys. Rev. Lett. 6(2), 47-48, 1961.

Farrugia, C. J., F. T. Gratton, G. Gnavi, R. B. Torbert, L. B. Wilson, A vortical dawn flank boundary layer for near-radial IMF: Wind observations on 24 October 2001, J. Geophys. Res. Space Physics, 119, 4572-4590, doi: 10.1002/2013JA019578, 2014.

Fujimoto, M., Terasawa, T., Mukai, T., Saito, Y., Yamamoto, T., and Kokubun, S.: Plasma entry from the flanks of the near-Earth magnetotail: Geotail observations, J. Geophys.Res. 103(A3), 4391-4408, 1998.

Fujimoto M., Tonooka, T., and Mukai, T.: Vortex-like fluctuations in the magnetotail flanks and their possible roles in plasma transport in the Earth's Low-Latitude Boundary Layer, Geophys. Monogr. Ser., vol. 133. Edited byNewell, P. T., and Onsager, T., p. 241, AGU., Washington D. C., 2003.

Grygorov, K., Němeček, Z., Šafránková, J., Přech, L., Pi, G., Shue, J.-H.: Kelvin-Helmholtz wave at the subsolar magnetopause boundary layer under radial IMF. J. Geophys., Res. Space Physics, 121, 9863-9879, doi: 10.1002/2016JA023068, 2016.

Hasegawa, A.: Plasma instabilities and Non-linear effects, Springer-Verlag, New York, 1975.

Hasegawa, H., Fujimoto, M., Phan, T.-D., Rème, H., Balogh, A., Dunlop, M. W., Hashimoto, C., and TanDokoro, R.: Transport of solar wind into Earth's magnetosphere through rolled-up Kelvin-Helmholtz vortices. Nature, 430, 755-758, doi:10.1038/nature02799, 2004.

Hasegawa, H., Fujimoto, M., Takagi, K., Saito, Y., Mukai, T., and Rème, H.: Single-spacecraft detection of rolled-up Kelvin-Helmholtz vortices at the flank magnetopause. J. Geophys. Res., 111, A09203, doi:10.1029/2006JA011728, 2006.

Hasegawa, H., Retinò, A., Vaivads, A., Khotyaintsev, Y., André, M., Nakamura, T. K. M., Teh, W. –L., Sonnerup, B. U. Ö., Schwartz, S. J., Seki, Y., Fujimoto, M., Saito, Y., Rème, H., and Canu, P.: Kelvin-Helmholtz waves at the Earth's magnetopause: Multiscale development and associated reconnection, J. Geophys. Res., 114, A12207, doi:10.1029/2009JA014042, 2009.

Hashmoto, C., and Fuijimoto, M.: Kelvin-Helmholtz instability in an unstable layer of finite thickness, Adv. Space Res., 37, 527, 2005.

Hwang, K.-J, Kuznetsova, M. M., Sahraoui, F., Goldstein, M. L., Lee, E., and Parks, G. K.: Kelvin-Helmholtz waves under southward interplanetary magnetic field, J. Geophys. Res., 116, A08210, doi:10.1029/2011JA016596, 2011.

https://doi.org/10.5194/angeo-2019-103
Preprint. Discussion started: 19 July 2019
© Author(s) 2019. CC BY 4.0 License.
Annales Geophysicae Discussions

Hwang, K.-J., Goldstein, M. L., Kuznetsova, M. M., Wang, Y., Vinas, A. F., and Sibeck, D. G.: The first in situ observation of Kelvin-Helmholtz waves at high-latitude magnetopause during stongly dawnward interplanetary magnetic field conditions, J. Geophys. Res., 117, A08233, doi: 10.1029/2011JA017256, 2012.

Johnson, J. R., Wing, S., Delamere, P. A.: Kelvin Helmholtz Instability in Planetary Magnetospheres, Space Sci. Rev., 184, 1-31, doi: 10.1007.s11214-014-0085-z, 2014.

Kavosi, S. and Raeder, J.: Ubiquity of Kelvin-Helmholtz waves at Earth's magnetopause. Nat. Commun., 6:7019, doi:10.1038/ncomms8019, 2015

Kawano, H., Kokubun, S., Yamamoto, Y., Tsuruda, K., Hayakawa, H., Nakamura, M., Okada, T., Matsuoka, A., and Nishida, A.: Magnetopause characteristics during a four-hour interval of multiple crossings observed with GEOTAIL, Geophys. Res. Lett., 21, 2895-2898, 1994.

Kivelson, M. G., and Chen, S. H.: The magnetopause: Surface waves and instabilities and their possible dynamic consequences, in Physics of the Magnetopause, Geophys. Monogr. Ser., vol. 90. Edited by Song, P., Sonnerup, B. O. Ü., and Thomsen, M. F., p. 257, AGU., Washington D. C., 1995.

Li, W. Y., André, M., Khotyaintsev, Y. V., Vaivads, A., Graham, D. B., Toledo-Redondo, S., and Strangeway, R. J.: Kinetic evidence of magnetic reconnection due to Kelvin-Helmholtz waves. Geophys. Res. Lett., 43, 5635-5643, doi: 10.1002/2016GL069192, 2016.

Manuel, J. R., and Samson, J. C.: The Spatial Development of the Low-latitude Boundary Layer. J. Geophys. Res., 98(A10), 17367-17385, 1993.

Masson, A., and Nykyri, K.: Kelvin-Helmholtz Instability: Lessons Learned and Ways Forward. 214, 71-89, doi:10.1007/s11214-018-0505-6, 2018.

Matsumoto Y., and Hoshino, M.: Onset of turbulence induced by a Kelvin-Helmholtz vortex. Geophys. Res. Lett., 31, L02807, doi: 10.1029/2003GL018195, 2004.

McFadden, J. P., Carlson, C. W., Larson, D., Ludlam, M., Abiad, R., Elliott, B., Turin, P., Marckwordt, M., and Angelopoulos, V.: The THEMIS ESA plasma instrument and in-flight calibration. Space Sci. Rev., 141, 277–302, doi:10.1007/s11214-008-9440-2, 2008.

Miura, A.: Dependence of the magnetopause Kelvin-Helmholtz instability on the orientation of the magnetosheath magnetic field. Geophys. Res. Lett., 22, 2993, 1995.

Moore, T. W., Nykyri, K., Dimmock, A. P.: Cross scale energy transport in space plasmas. Nat. Phys., 12, 1164-1169, doi: 10.1038/nphys3869, 2016.

Mozer, F. S., Hayakawa, H., Kokubun, S., Nakamura, M., Okada, T., Yamamoto, T., and Tsuruda, K.: The morningside low-latitude boundary layer as determined from electric field and magnetic field measurements on Geotail, Geophys. Res. Lett., 21, 2983, 1994.

Nakamura, T. K. M., Hayashi, D., and Fujimoto, M.: Decay of MHD-Scale Kevin-Helmholtz Vortices Mediated by Parasitic Electron Dynamics. Phys. Rev Lett., 92(14), 145001, doi: 10.1103/PhysRevLett.92.14501, 2004.

Nakamura, T. K. M., Eriksson, S., Hasegawa, H., Zenitani, S., Li, W. Y., Genestreti, K. J., Nakamura, R., and Daughton, W.: Mass and Energy Transfer across the Earth's Magnetopause Caused by Vortex-Induced Reconnection, J. Geophys. Res.: Space Physics, 122, 11505-11522, doi: 10.1002/2017JA024346, 2017.

Nykyri, K., and Otto, A.: Plasma transport at the magnetospheric boundary due to reconnection in Kelvin-Helmholtz vortices, Geophys. Res. Lett., 28, 3565-3568, 2001.

Nykyri, K., Otto, A., Lavraud, B., Mouikis, C., Kistler, L. M., Balogh, A., and Rème, H.:

https://doi.org/10.5194/angeo-2019-103
Preprint. Discussion started: 19 July 2019
© Author(s) 2019. CC BY 4.0 License.



Cluster observations of reconnection due to the Kelvin-Helmholtz instability at the dawnside magnetosphere flank, Ann. Geophys., 24, 2619-2643, 2006.

Otto, A, and Fairfield, D. H.: Kelvin-Helmholtz instability at the magnetotail boundary: MHD simulation and comparison with Geotail observations, J. Geophys. Res., 105(A9), 21175-21190, 2000.

Shue, J.-H., Song, P., Russell, C. T, Steinberg, J. T., Chao, J. K., Zastenker, G., Vaisberg, O. L., Kokubun, S., Singer, H. J., Detman, T. R., and Kawano, H.: Magnetopause location under extreme solar wind conditions, J. Geophys. Res., 103, 17691-17700, 1998.

Sibeck, D. G.: Transient event in the Outer magnetosphere: boundary waves or flux transfer event? J. Geophys. Res., 97(A4), 4009-4026, 1992.

Sckopke, N., Paschmann, G., Haerendel, G., Sonnerup, B. U. Ö., Bame, S. J., Forbes, T. G., Hones Jr, E. W., andRussell, C. T.: Structure of the Low- Latitude Boundary Layer, J. Geophys. Res., 86(A4), 2099-2110, 1981.

Sonnerup, B. U. Ö., and Cahill, L. J.: Of the magnetopause current layer, J. Geophys. Res., 73, 1757-1770, 1968.

Song P., and Russell, C. T.: Model of the formation of the low-latitude-boundary-layer for strongly northward interplanetary magnetic field, J. Geophys. Res., 97(A2), 1411-1420, doi, 10.1029/91JA02377, 1992.

Southwood, D. J.: Magnetopause Kelvin-Helmholtz instability, in Magnetosphere Boundary Layers, edited by Battrick, B., and Mort, J., pp. 357-364, European Space Agency Scientific and Technical Publications Branch, Noordwijk, The Netherlands, 1979.

Tang, B. B., Wang, C., and Li, W. Y.: The magnetosphere under the radial interplanetary magnetic field: A numerical study, J. Geophys., Res. Space Physics, 118, 7674-7682, doi: 10.1002/2013JA019155, 2013.

Walsh, B. M., Thomas, E. G., Hwang, K. -H., Baker, J. B. H., Ruohoniemi, J. M., Bonnell, J. W.: Dense plasma and Kelvin-Helmholtz waves at Earth's dayside magnetopause, J. Geophys. Res.: Space Physics, 120, 5560-5573, doi: 10. 1002/2015JA021014, 2015.

Yan, G. Q., Shen, C., Liu, Z. X., Rème, H., Carr, C. M., and Zhang, T. L.: A Statistical Study on Correlations between Plasma Sheet and Solar Wind Based on DSP Explorations, Ann. Geophys., 23, 2961-2966, 2005.

Yan, G. Q., Mozer, F. S., Shen, C., Chen, T., Parks, G. K., Cai, C. L., McFadden, J. P.: Kelvin-Helmholtz Vortices observed by THEMIS at the duskside of the magnetopause under southward IMF. Geophys. Res. Lett., 41, 4427-4434, doi:10.1002/2014GL060589, 2014.

https://doi.org/10.5194/angeo-2019-103
Preprint. Discussion started: 19 July 2019
© Author(s) 2019. CC BY 4.0 License.

Annales Geophysicae
Discussions
Open Access

Figures and Captions

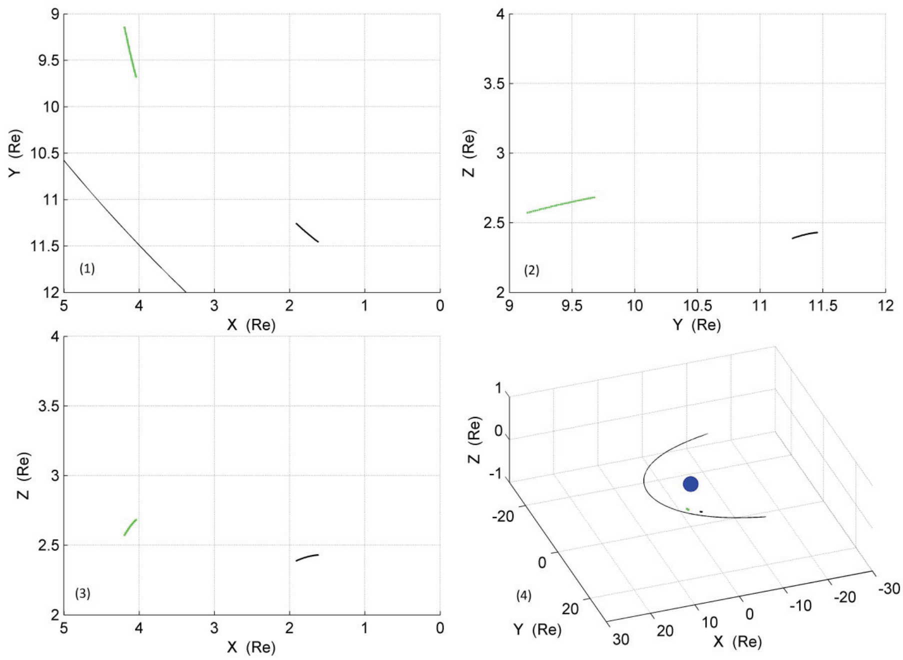


Figure 1. The orbits and positions of TH-A (green) and TH-E (black) during the interval of interest UT 22:20 ~ UT 22:54. The position data are expressed in GSM coordinates.

https://doi.org/10.5194/angeo-2019-103
Preprint. Discussion started: 19 July 2019
© Author(s) 2019. CC BY 4.0 License.
Annales Geophysicae
Discussions
Open Access

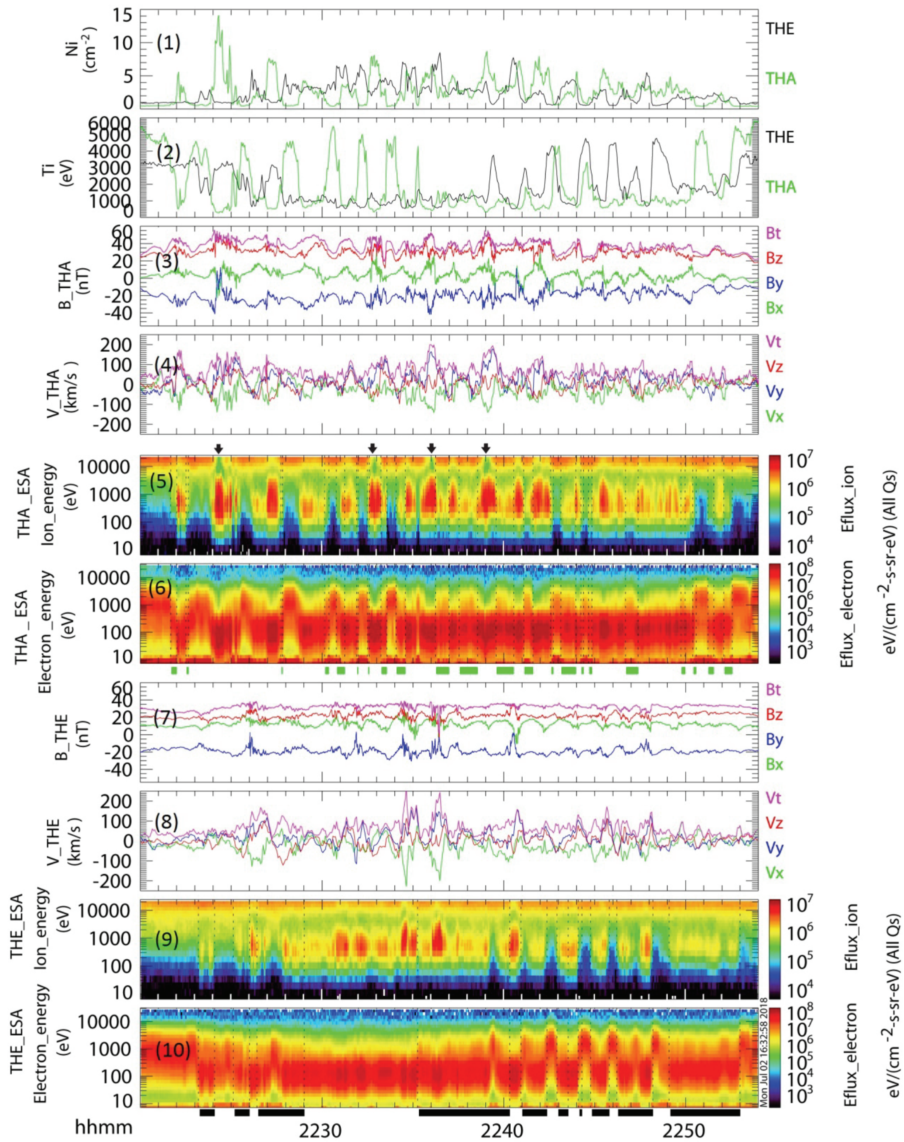


Figure 2. Fluctuations in the plasma parameters and the ion and electron energy-time spectra. Panel 1 is the ion densities from TH-A as a green line and from TH-E as a black line; panel 2 is the ion temperatures from TH-A as a green line and from TH-E as a black line; panels 3 and 4 are the magnetic field vectors and the ion bulk velocity vectors from TH-A, respectively; panels 5 and 6 are the ion and electron energy-time spectra from TH-A, respectively; panels 7 and 8 are the magnetic field vectors and the ion bulk velocity vectors from TH-E, respectively; panels 9 and 10 are the ion and electron energy-time spectra from TH-E, respectively. Vectors are all expressed in GSM coordinates.

https://doi.org/10.5194/angeo-2019-103
Preprint. Discussion started: 19 July 2019
© Author(s) 2019. CC BY 4.0 License.
Annales Geophysicae
Discussions
Open Access

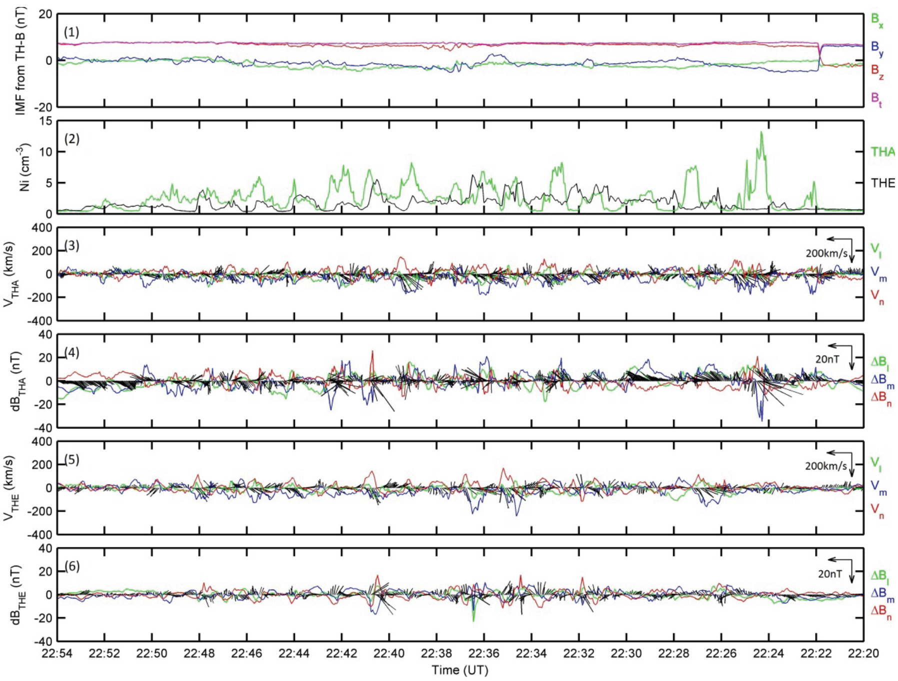


Figure 3. The observed plasma rotations and stretching of the magnetic field lines because of the formation of K-H vortices. Panel 1 is the IMF monitored by TH-B near the lunar orbit, with a time lag of 10 minutes from subsolar magnetopause to TH-B; panel 2 are the ion densities from TH-A in green and from TH-E in black; panels 3 and 5 are the ion bulk velocities from TH-A and TH-E, respectively, expressed in averaged local magnetopause coordinates LMN, deduced from the magnetopause model (Shue et al., 1998); panels 4 and 6 are the magnetic field deviations, $\Delta\boldsymbol{B}=\boldsymbol{B}-\boldsymbol{B}_{mean}$, from TH-A and TH-E respectively, expressed in LMN. Note that the time begins from the right and passes to the left.

https://doi.org/10.5194/angeo-2019-103
Preprint. Discussion started: 19 July 2019
© Author(s) 2019. CC BY 4.0 License.

Annales Geophysicae Discussions
Open Access

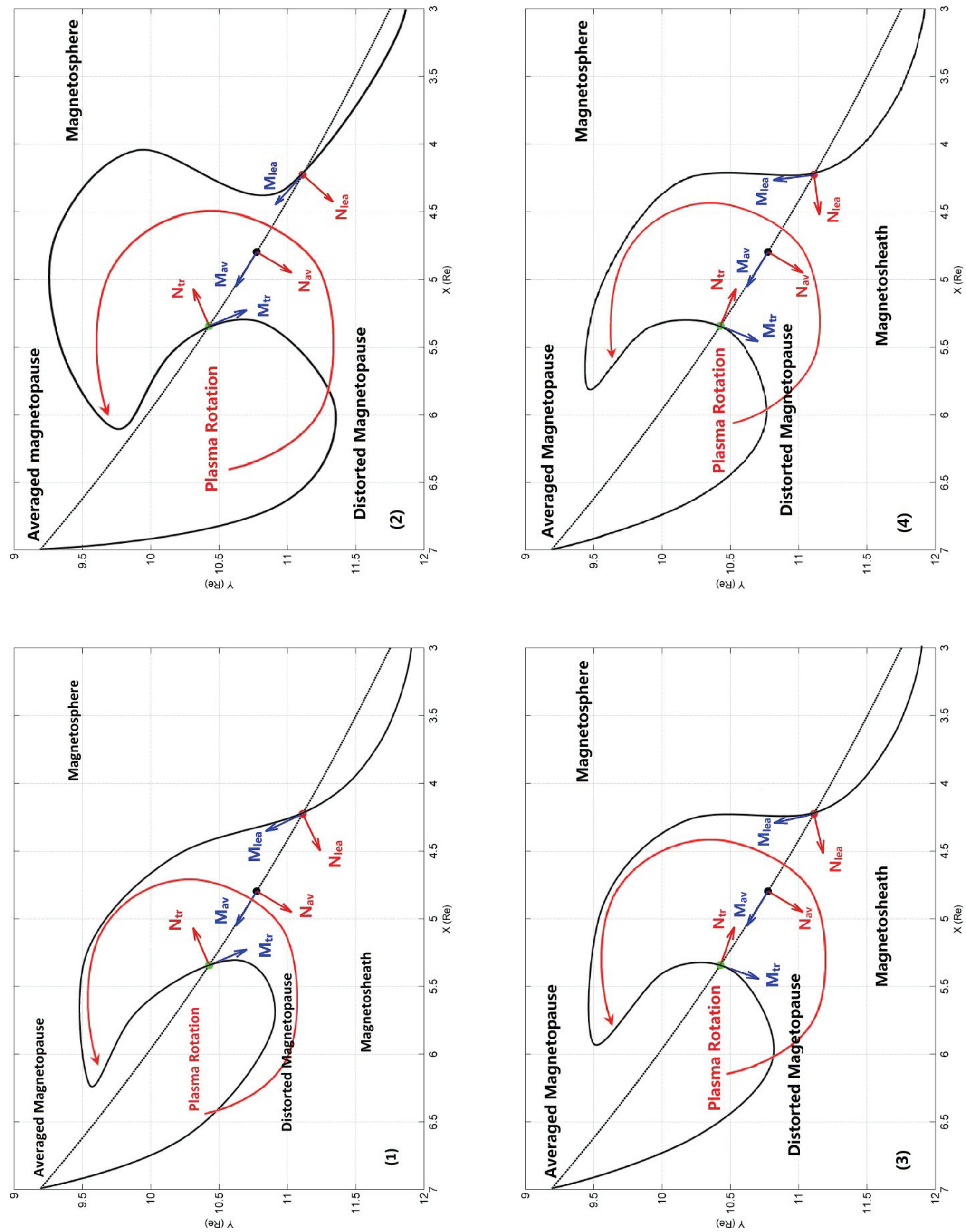

https://doi.org/10.5194/angeo-2019-103
Preprint. Discussion started: 19 July 2019
© Author(s) 2019. CC BY 4.0 License.

Annales Geophysicae Discussions

Figure 4. The magnetopause distortions formed by the K-H vortices deduced by the MVA. The average magnetopause (dashed lines), approximated to the spacecraft trajectory, was calculated from the magnetopause model (Shue et al., 1998). Traversal pair at UT 22:24 in panel 1: $M_{lea}$=(0.4374, -0.8141, -0.3819) and $N_{lea}$=(0.8970, 0.4251, 0.1212) at the outbound crossing; $M_{tr}$=(-0.3877, 0.8830, 0.2645) and $N_{tr}$=(-0.9195, -0.3906, -0.0438) at the inbound crossing. Traversal pair at UT 22:32 in panel 2: $M_{lea}$=(0.8349, -0.3995, -0.3786) and $N_{lea}$=(0.5504, 0.6081, 0.5721) at the outbound crossing; $M_{tr}$=(-0.3946, 0.8595, -0.3248) and $N_{tr}$=(-0.9171, -0.3900, 0.0821) at the inbound crossing. Traversal pair at UT 22:36 in panel 3: $M_{lea}$=(0.1004, -0.8420, -0.5301) and $N_{lea}$=(0.9594, 0.2231, -0.1726) at the outbound crossing; $M_{tr}$=(0.3363, 0.9417, -0.0076) and $N_{tr}$=(-0.9417, 0.3362, -0.0135) at the inbound crossing. Traversal pair at UT 22:39 in panel 4: $M_{lea}$=(0.0363, -0.9014, -0.4314) and $N_{lea}$=(0.9724, 0.1315, -0.1930) at the outbound crossing; $M_{tr}$=(-0.5073, -0.5145, -0.6913) and $N_{tr}$=(-0.8599, 0.3556, 0.3662) at the inbound crossing.

https://doi.org/10.5194/angeo-2019-103
Preprint. Discussion started: 19 July 2019
© Author(s) 2019. CC BY 4.0 License.

Annales Geophysicae
Open Access
Discussions
EGU

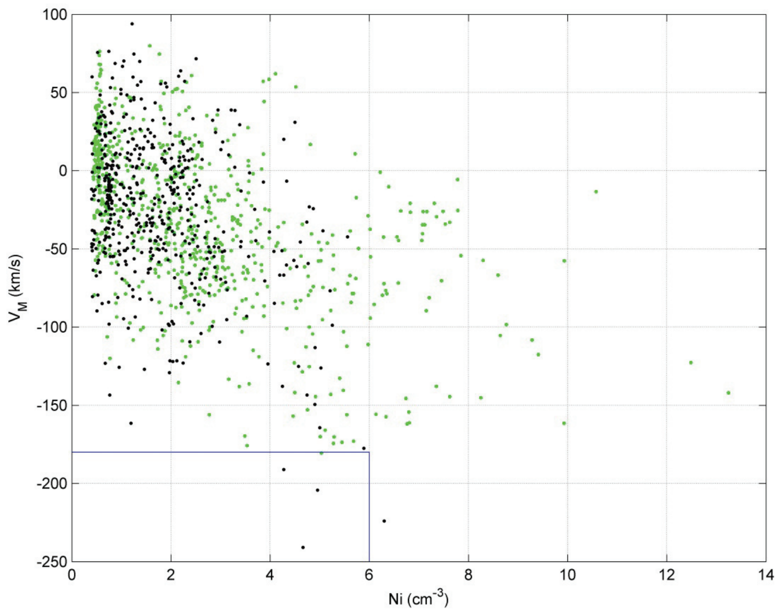


Figure 5. The observed velocity along the tailward direction versus the ion density. Green dots are from TH-A observations and black dots from TH-E observations. The blue lines mark the high-speed and low density region possibly caused by the acceleration of the rotation.

https://doi.org/10.5194/angeo-2019-103
Preprint. Discussion started: 19 July 2019
© Author(s) 2019. CC BY 4.0 License.
Annales Geophysicae Discussions

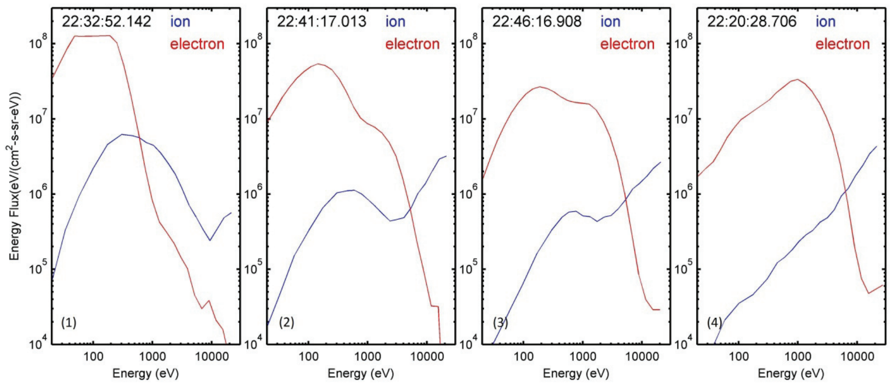


Figure 6. Typical portraits of the energy-time spectra of plasmas in different regions. Panel 1 is the magnetosheath observed by TH-A at 22:32:52.142; panel 2 is mixture region I observed by TH-A at 22:41:17.013; panel 3 is mixture region II observed by TH-E at 22:46:16.908; panel 4 is the magnetosphere observed by TH-A at 22:20:28.706.